

Adversarial Random Forests for Density Estimation and Generative Modelling

David S. Watson^{1*}, Kristin Blesch^{2,3}, Jan Kapar^{2,3}, Marvin N. Wright^{2,3,4}

¹Department of Informatics, King’s College London, London, UK

²Leibniz Institute for Prevention Research & Epidemiology – BIPS, Bremen, Germany

³Faculty of Mathematics and Computer Science, University of Bremen, Bremen, Germany

⁴Department of Public Health, University of Copenhagen, Copenhagen, Denmark

*Corresponding author: David S. Watson; david.watson@kcl.ac.uk

Abstract

We propose methods for density estimation and data synthesis using a novel form of unsupervised random forests. Inspired by generative adversarial networks, we implement a recursive procedure in which trees gradually learn structural properties of the data through alternating rounds of generation and discrimination. The method is provably consistent under minimal assumptions. Unlike existing tree-based alternatives, our approach provides smooth unconditional densities and allows for fully synthetic data generation. We achieve comparable or superior performance to state-of-the-art deep learning models on various tabular data benchmarks while executing about two orders of magnitude faster on average. All algorithms are implemented in easy-to-use R and Python packages.

1 Introduction

Density estimation is a fundamental unsupervised learning task, an essential subroutine in various methods for data imputation [28, 71], clustering [11, 69], anomaly detection [16, 59], and classification [50, 85]. One important application for density estimators is generative modeling, where we aim to create synthetic samples that mimic the characteristics of real data. These simulations can be used to test the robustness of classifiers [79, 15], augment training sets with synthetic samples [68, 49], or study complex systems without compromising the privacy of data subjects [4, 94].

The current state of the art in generative modeling relies on deep neural networks, which have proven remarkably adept at synthesizing images, audio, and even video data. Architectures built on variational autoencoders (VAEs) [42] and generative adversarial networks (GANs) [36] have dominated the field for the last decade. Recent advances in normalizing flows [60] and diffusion models [67] have sparked considerable interest. While these algorithms are highly effective with structured data, they can struggle in tabular settings with continuous and categorical covariates. Even when successful, deep learning models are notoriously data-hungry and require extensive tuning.

We introduce an adversarial random forest algorithm that vastly simplifies the task of density estimation and data synthesis. Our method naturally accommodates mixed data in tabular settings, and performs well on small and large datasets using the computational resources of a standard laptop. It is more accurate than leading tree-based alternatives and about 100 times faster than deep learning solutions, with little or no tuning required.

Following a brief discussion of related work (Sect. 2), we review relevant notation and background on random forests (Sect. 3). We motivate our method with theoretical results that guarantee convergence under reasonable assumptions (Sect. 4), and illustrate its performance on a range of benchmark tasks (Sect. 5). We conclude with a discussion (Sect. 6) and directions for future work (Sect. 7).

2 Related Work

A random forest (RF) is a bootstrap-aggregated (bagged) ensemble of independently randomized trees [12], typically built using the greedy classification and regression tree (CART) algorithm [14]. RFs are extremely popular and effective, widely used in areas like bioinformatics [17], remote sensing [6], and

ecology [21], as well as more generic prediction tasks [30]. Advantages include their efficiency (RFs are embarrassingly parallelizable), ease of use (they require minimal tuning), and ability to adapt to sparse signals (uninformative features are rarely selected for splits).

It is well-known that tree-based models can approximate joint distributions. Several authors advocate using leaf nodes of CART trees as piecewise constant density estimators [65, 91, 89]. While this method provably converges on the true density in the limit of infinite data, finite sample performance is inevitably rough and discontinuous. Smooth results can be obtained by applying either kernel density estimation (KDE) or maximum likelihood estimation (MLE) within each leaf [78, 38, 48, 65, 20, 19], a version of which we develop further below. Existing methods have mostly been limited to supervised trees rather than unsupervised forests, and are inefficient with more than a handful of covariates.

Another strategy, better suited to high-dimensional data, uses Chow-Liu trees to learn a second-order approximation to the underlying joint distribution [5, 47, 64]. Whereas these methods estimate a series of bivariate densities over the full support of the data, we reduce complexity even further, computing univariate densities in smaller subregions.

Despite the popularity of tree-based density estimators, they are rarely if ever used for fully synthetic data generation. Instead, they are commonly used for *conditional* density estimation and data imputation [81, 82, 19, 51]. We highlight that methods optimized for this task are often ill-suited to generative modeling, since their reliance on supervised signals limits their ability to capture dependencies between features with little predictive value for the selected outcome variable(s).

The contemporary literature on generative models arguably begins with the introduction of VAEs [42] and GANs [36], which jointly optimize parameters for network pairs—encoder-decoder and generator-discriminator, respectively—via stochastic gradient descent. Various extensions of these approaches have been developed [39, 2], including some designed for mixed data in the tabular setting [18, 40, 92]. While the evidence lower bound of a VAE approximates the data likelihood, there is no straightforward way to compute this quantity with GANs. More recent work in neural density estimation includes autoregressive networks [83, 66, 70], normalizing flows [44, 60, 46], and diffusion models [43, 80, 67]. These methods are generally optimized for structured data such as images or audio, where they often attain state-of-the-art results.

3 Background

Consider the binary classification setting with training data $\mathcal{D} = \{(\mathbf{x}_i, y_i)\}_{i=1}^n$, where $\mathbf{x}_i \in \mathcal{X} \subset \mathbb{R}^d$ and $y_i \in \mathcal{Y} = \{0, 1\}$. Samples are independent and identically distributed according to some fixed but unknown distribution P with density p . The classic RF algorithm takes B bootstrap samples of size n from \mathcal{D} and fits a binary decision tree for each, in which observations are recursively partitioned according to some optimization target (e.g., Gini index) evaluated on a random subset of features at each node. The size of this subset is controlled by the `mtry` parameter, conventionally set at $\lfloor \sqrt{d} \rfloor$ for classification. Resulting splits are literals of the form $X_j \bowtie x$ for some $X_j, j \in [d] = \{1, \dots, d\}$, and value $x \in \mathcal{X}_j$, where $\bowtie \in \{=, <\}$ (the former for categorical, the latter for continuous variables). Data pass to left or right child nodes depending on whether they satisfy the literal. Splits continue until some stopping criterion is met (e.g., purity). Terminal nodes, a.k.a. *leaves*, describe hyperrectangles in feature space with boundaries given by the learned splits. These disjoint cells collectively cover all of \mathcal{X} . Each leaf is associated with a label $\hat{y} \in [0, 1]$, representing either the frequency of positive outcomes (soft labels) or the majority class (hard labels) within that cell. Because trees are grown on independent bootstraps, an average of n/e samples are excluded from each tree. This so-called “out-of-bag” (OOB) data can be used to estimate empirical risk without need for cross-validation.

Each new datapoint \mathbf{x} falls into exactly one leaf in each tree. Predictions are computed by aggregating over the trees, e.g. by tallying votes across all B basis functions of the ensemble. Let θ_b^ℓ denote the conjunction of literals that characterize membership in leaf $\ell \in [L_b]$, where L_b is the number of leaves in tree $b \in [B]$, with corresponding hyperrectangular subspace $\mathcal{X}_b^\ell \subset \mathcal{X}$. Let n_b be the number of training samples for tree b , and n_b^ℓ the number of samples that fall into leaf ℓ of b . The ratio n_b^ℓ/n_b represents an empirical estimate of the leaf’s coverage $p(\theta_b^\ell)$, i.e. the probability that a random \mathbf{x} falls within \mathcal{X}_b^ℓ . A tree is fully parametrized by $\theta_b = \bigcup_{\ell=1}^{L_b} \theta_b^\ell$, and the complete forest by $\Theta = \bigcup_{b=1}^B \theta_b$.

Our method builds on the *unsupervised* random forest (URF) algorithm [75, 1, 53]. This procedure creates a synthetic dataset $\tilde{\mathbf{X}}$ of n observations by independently sampling from the marginals of \mathbf{X} , i.e. $\tilde{\mathbf{x}} \sim \prod_{j=1}^d P(X_j)$. A RF classifier is trained to distinguish between \mathbf{X} and $\tilde{\mathbf{X}}$, with labels indicating whether samples are original ($Y = 1$) or synthetic ($Y = 0$). The method has expected accuracy 1/2 in the worst case, corresponding to a dataset in which all features are mutually independent. However, if true

Algorithm 1 ADVERSARIAL RANDOM FOREST

Input: Training data $\mathbf{X} \in \mathbb{R}^{n \times d}$, tolerance δ

Output: Random forest classifier $f^{(0)}$

```
Sample  $\tilde{\mathbf{X}}^{(0)} \sim \prod_{j=1}^d P(X_j)$ 
 $\mathbf{X}^+ \leftarrow \text{row.append}(\mathbf{X}, \tilde{\mathbf{X}}^{(0)})$ 
 $Y \leftarrow \text{row.append}(\mathbf{1}_n, \mathbf{0}_n)$ 
 $f^{(0)} \leftarrow \text{RANDOMFOREST}(\mathbf{X}^+, Y)$ 
if  $\text{ACC}(f^{(0)}) > 1/2 + \delta$  then
  converged  $\leftarrow$  FALSE
  while not converged do
    for all  $b \in [B], \ell \in [L_b]$  do
       $q(\theta_b^\ell) \leftarrow \frac{1}{2n_b} \sum_{i: \mathbf{x}_i \in \mathcal{X}_b^\ell} y_i$ 
    end for
    for  $i \in [n]$  do
      Sample tree  $b \in [B]$  uniformly
      Sample leaf  $\ell \in [L_b]$  w.p.  $q(\theta_b^\ell)$ 
      Sample  $\tilde{\mathbf{x}}_i^{(1)} \sim \prod_{j=1}^d P(X_j | \theta_b^\ell)$ 
    end for
     $\mathbf{X}^+ \leftarrow \text{row.append}(\mathbf{X}, \tilde{\mathbf{X}}^{(1)})$ 
     $f^{(1)} \leftarrow \text{RANDOMFOREST}(\mathbf{X}^+, Y)$ 
    if  $\text{ACC}(f^{(1)}) \leq 1/2 + \delta$  then
      converged  $\leftarrow$  TRUE
    else
       $f^{(0)} \leftarrow f^{(1)}$ 
    end if
  end while
end if
```

accuracy converges to $1/2 + \delta$ for some $\delta > 0$, then consistent testing procedures will almost surely detect the discrepancy as n grows [41].

4 Adversarial Random Forests

We introduce a recursive variant of URFs, which we call *adversarial random forest* (ARF). The goal of this algorithm is to render data jointly independent within each leaf. We achieve this by first fitting an ordinary URF $f^{(0)}$ with synthetic data $\tilde{\mathbf{X}}^{(0)}$. We compute the coverage of each leaf w.r.t. original data, then generate a new synthetic dataset by sampling from marginals within random leaves selected with probability proportional to this coverage. Call the resulting $n \times d$ matrix $\tilde{\mathbf{X}}^{(1)}$. A new classifier $f^{(1)}$ is trained to distinguish \mathbf{X} from $\tilde{\mathbf{X}}^{(1)}$. If OOB accuracy for this model is sufficiently low, then the ARF has converged, and we move forward with splits from $f^{(0)}$. Otherwise, we iterate the procedure, drawing a new synthetic dataset from the splits learned by $f^{(1)}$ and evaluating performance via a new classifier. The loop repeats until convergence (see Alg. 1).

ARFs bear some obvious resemblance to GANs. The “generator” is a simple sampling scheme that draws from the marginals in adaptively selected subregions; the “discriminator” is an RF classifier. The result can be understood as a zero-sum game in which adversaries take turns increasing and decreasing label uncertainty at each round. However, beyond this conceptual link between our method and GANs lie some important differences. Both generator and discriminator share the same parameters in our algorithm. Indeed, our generator does not, strictly speaking, *learn* anything; it merely exploits what the discriminator has learned. This means that ARFs cannot be used for adversarial attacks of the sort made famous by GANs, which involve separately parametrized networks for each model. Moreover, the synthetic data generated by ARFs is relatively naive, consisting of bootstrap samples drawn from subsets of the original observations. That is because our goal is not (yet) to generate new data, but merely to learn an independence-inducing partition. Empirically, we find that this is often achieved in just a single round even for $\delta = 0$.

Formally, we seek a set of splits Θ such that, for all trees b , leaves ℓ , and samples \mathbf{x} , we have $p(\mathbf{x} | \theta_b^\ell) = \prod_{j=1}^d p(x_j | \theta_b^\ell)$. We call this the *local independence criterion*. Our first result states that ARFs converge on this identity in the limit. Following a common trend in the literature [54, 7, 23, 74, 55, 86, 3, 61],

we consider a slightly modified version of the RF algorithm for analysis. Predictions are made with the soft labeling approach described above. We assume:

- (A1) The domain of \mathbf{X} is limited to the unit hypercube, $\mathcal{X} = [0, 1]^d$, and its density p is bounded away from 0 and ∞ .
- (A2) At each iteration of the ARF algorithm, the target function $P(Y = 1|\mathbf{x})$ is Lipschitz-continuous.
- (A3) Trees are honest and regular, as defined by Wager and Athey [86]. That is, (i) training data for each tree is split into two subsets: one to learn split parameters, and the other to assign leaf labels; (ii) every split puts at least $\gamma \in (0, 0.2]$ of the available observations into each child node; (iii) at each internal node, the probability that the tree splits on any given X_j is bounded from below by some $\pi > 0$; (iv) the subsample size satisfies $n_b \rightarrow \infty$ and $n_b \log(n)^d/n \rightarrow 0$; (v) the leaf size satisfies $\min_{\ell, b} (n_b^\ell) \rightarrow \infty$.

(A1) is simply for notational convenience, and can be replaced w.l.o.g. by bounding the domain of \mathbf{X} with arbitrary constants. (A2) is a common learning theoretic assumption widely used in the analysis of RFs [54, 7, 32]. The tree specification conditions of (A3) were originally introduced in the context of RF regression analysis [86]. For reasons explained in Appx. A, they are better suited to our purpose than alternative consistency conditions reported for RF classifiers.

Theorem 1 (Convergence). *Under assumptions (A1)-(A3), ARFs almost surely satisfy the local independence criterion as sample size grows:*

$$\forall \ell \forall \mathbf{x} : \mathbb{P} \left[\lim_{n \rightarrow \infty} p(\mathbf{x}|\theta^\ell) = \prod_{j=1}^d p(x_j|\theta^\ell) \right] = 1,$$

where ℓ ranges over the set \mathcal{L} of all possible axis-aligned splits on \mathcal{X} .

See Appx. A for all proofs.

4.1 Density Estimation and Data Synthesis

ARFs are the core subroutine behind FORests for Density Estimation (FORDE) and FORests for GEnerative modeling (FORGE). We present pseudocode for both algorithms (see Algs. 2 and 3). The key point to recognize is that, under the local independence criterion, joint densities can be learned by running d separate univariate estimators within each leaf. This is exponentially easier than multivariate density estimation, which suffers from the notorious *curse of dimensionality*. Summarizing the challenges with estimating joint densities, one recent textbook on KDE concludes that “nonparametric methods for kernel density problems should not be used for high-dimensional data and it seems that a feasible dimensionality should not exceed five or six...” [37, p. 60]. By contrast, our method scales much better with data dimensionality, exploiting the flexibility of ARFs to learn an independence-inducing partition that renders density estimation relatively straightforward.

Of course, this does not *escape* the curse of dimensionality so much as relocate it. The cost for this move is potentially deep trees and/or many ARF training rounds, especially when dependencies between covariates are strong or complex. However, deep forests are generally more efficient than deep neural networks in terms of data and computation, and our experiments suggest that ARF convergence is usually fast even for $\delta = 0$ (see Sect. 5).

With our ARF in hand, the algorithm proceeds as follows. For each tree b , we record the split criteria θ_b^ℓ and empirical coverage $q(\theta_b^\ell)$ of each leaf ℓ . Call these the *leaf parameters*. Then we estimate *distribution parameters* $\psi_{b,j}^\ell$ independently for each (original) X_j within \mathcal{X}_b^ℓ , e.g. the kernel bandwidth for KDE or class probabilities for MLE with categorical data. In the continuous case, $\psi_{b,j}^\ell$ must either encode leaf bounds (e.g., via a truncated normal distribution with extrema given by θ_b^ℓ) or include a normalization constant to ensure integration to unity. The generative model then follows a simple two-step procedure. First, sample a tree uniformly from $[B]$ and a leaf from that tree with probability $q(\theta_b^\ell)$, just as we do to construct synthetic data within the recursive loop of the ARF algorithm. Next, sample data for each feature X_j according to the density/mass function parametrized by $\psi_{b,j}^\ell$. We repeat this procedure until the target number of synthetic samples has been generated.

We are deliberately agnostic about how distribution parameters $\psi_{b,j}^\ell$ should be learned, as this will tend to vary across features. In our theoretical analysis, we restrict focus to continuous variables and consider a flexible family of KDE methods. For our experiments, we use MLE, assuming local normality for

Algorithm 2 FORDE

Input: ARF classifier f , training data $\mathbf{X} \in \mathbb{R}^{n \times d}$

Output: Estimated density q

for all $b \in [B], \ell \in [L_b]$ **do**

$$q(\theta_b^\ell) \leftarrow \frac{1}{2n_b} \sum_{i: \mathbf{x}_i \in \mathcal{X}_b^\ell} y_i$$

for $j \in [d]$ **do**

$\psi_{b,j}^\ell \leftarrow$ estimated parameter(s) for $p(x_j | \theta_b^\ell)$

$q(\cdot; \psi_{b,j}^\ell) \leftarrow$ corresponding pdf/pmf

end for

end for

Algorithm 3 FORGE

Input: FORDE model q , target sample size m

Output: Synthetic dataset $\tilde{\mathbf{X}} \in \mathbb{R}^{m \times d}$

for $i \in [m]$ **do**

Sample tree $b \in [B]$ uniformly

Sample leaf $\ell \in [L_b]$ w.p. $q(\theta_b^\ell)$

for $j \in [d]$ **do**

Sample data $\tilde{x}_{ij} \sim q(\cdot; \psi_{b,j}^\ell)$

end for

end for

continuous data (effectively implementing a Gaussian mixture model), and computing class probabilities for categorical variables. Both techniques work well in practice. We revisit this issue in Sect. 6.

Our estimated density takes the following form:

$$q(\mathbf{x}) = \frac{1}{B} \sum_{\ell, b: \mathbf{x} \in \mathcal{X}_b^\ell} q(\theta_b^\ell) \prod_{j=1}^d q(x_j; \psi_{b,j}^\ell). \quad (1)$$

Compare this with the true density:

$$p(\mathbf{x}) = \frac{1}{B} \sum_{\ell, b: \mathbf{x} \in \mathcal{X}_b^\ell} p(\theta_b^\ell) p(\mathbf{x} | \theta_b^\ell). \quad (2)$$

In both cases, the density evaluated at a given point is just a coverage-weighted average of its density in all leaves whose split criteria it satisfies.

Because we are concerned with L_2 -consistency, our loss function is the mean integrated squared error (MISE)¹, defined as:

$$\text{MISE}(p, q) := \mathbb{E} \left[\int_{\mathcal{X}} (p(\mathbf{x}) - q(\mathbf{x}))^2 d\mathbf{x} \right].$$

We require one extra assumption, imposing standard conditions for KDE consistency [77]:

(A4) The true density function p is smooth. Specifically, its second derivative p'' is finite, continuous, square integrable, and ultimately monotone.

Our method admits three potential sources of error, quantified by the following residuals:

$$\epsilon_1 := \epsilon_1(\ell, b) := p(\theta_b^\ell) - q(\theta_b^\ell) \quad (3)$$

$$\epsilon_2 := \epsilon_2(\ell, b, \mathbf{x}) := \prod_{j=1}^d p(x_j | \theta_b^\ell) - \prod_{j=1}^d q(x_j; \psi_{b,j}^\ell) \quad (4)$$

$$\epsilon_3 := \epsilon_3(\ell, b, \mathbf{x}) := p(\mathbf{x} | \theta_b^\ell) - \prod_{j=1}^d p(x_j | \theta_b^\ell) \quad (5)$$

¹Alternative loss functions may also be suitable, e.g. information theoretic measures like the Kullback-Leibler divergence or integral probability metrics such as the Wasserstein distance.

We refer to these as errors of *coverage*, *density*, and *convergence*, respectively. Observe that ϵ_1 is a random variable that depends on ℓ and b , while ϵ_2, ϵ_3 are random variables depending on ℓ, b and \mathbf{x} . We drop the dependencies for ease of notation.

Lemma 1. The error of our estimator satisfies the following bound:

$$\text{MISE}(p, q) \leq 2B^{-2} \mathbb{E} \left[\int_{\mathcal{X}} \alpha^2 + \beta^2 d\mathbf{x} \right],$$

where

$$\begin{aligned} \alpha &:= \sum_{\ell, b: \mathbf{x} \in \mathcal{X}_b^\ell} p(\theta_b^\ell) \epsilon_3 \quad \text{and} \\ \beta &:= \sum_{\ell, b: \mathbf{x} \in \mathcal{X}_b^\ell} \left(p(\theta_b^\ell) \epsilon_2 + \epsilon_1 \prod_{j=1}^d p(x_j | \theta_b^\ell) - \epsilon_1 \epsilon_2 \right). \end{aligned}$$

This lemma establishes that total error is bounded by a quadratic function of $\epsilon_1, \epsilon_2, \epsilon_3$. We know by Thm. 1 that errors of convergence vanish in the limit. Our next result states that the same holds for errors of coverage and density.

Theorem 2 (Consistency). *Under assumptions (A1)-(A4), FORDE is L_2 -consistent. That is, the following holds almost surely: $\lim_{n \rightarrow \infty} \text{MISE}(p, q) = 0$.*

Our consistency proof is fundamentally unlike those of piecewise constant density estimators with CART trees [65, 91, 19], which essentially treat base learners as adaptive histograms and rely on tree-wise convergence when leaf volume goes to zero [24, 50]. Alternative methods that perform KDE or MLE within each leaf do not come with theoretical guarantees [78, 38, 48, 65]. Such algorithms are typically designed for *conditional* density estimation, and therefore require some outcome variable(s). This means that dependencies between features with little predictive value may be ignored, since trees are unlikely to split on them during model training. In the rare case that authors use some form of unsupervised splits, they make no effort to factorize the distribution and are therefore subject to the curse of dimensionality [20, 29]. By contrast, our method exploits ARFs to find regions of local independence, and univariate density estimation to compute marginals within each leaf. Though our consistency result comes at the cost of some extra assumptions, we argue that this is a fair price to pay for improved performance in finite samples.

5 Experiments

In this section, we present results from a wide range of experiments conducted on simulated and real-world datasets. In all cases, we use the default ARF parameters of 10 trees with a leaf size of 5 and $\text{mtreey} = \lfloor \sqrt{d} \rfloor$. For more details on hyperparameters, see Appx. B. Code for reproducing all results is included in the supplement; a link to a dedicated GitHub repository will be included following de-anonymization.

5.1 Simulation

FORGE recreates visual patterns. We begin with a simple proof of concept experiment, illustrating our method on a handful of low-dimensional datasets that allow for easy visual assessment. The `cassini`, `shapes`, `smiley`, and `twomoons` problems are all three-dimensional examples that combine two continuous covariates with a categorical class label. We simulate $n = 2,000$ samples from each data generating process (see Fig. 1, top row) and estimate densities using FORDE. We proceed to FORGE a synthetic dataset of $n = 2,000$ samples (Fig. 1, bottom row) and compare results. We find that the model consistently approximates its target distribution with high fidelity. Classes are clearly distinguished in all cases, and the visual form of the original data is immediately recognizable. Boundaries are not always crisp, especially in the `shapes` dataset. We hypothesize that this can be mitigated with more trees and/or a larger training set.

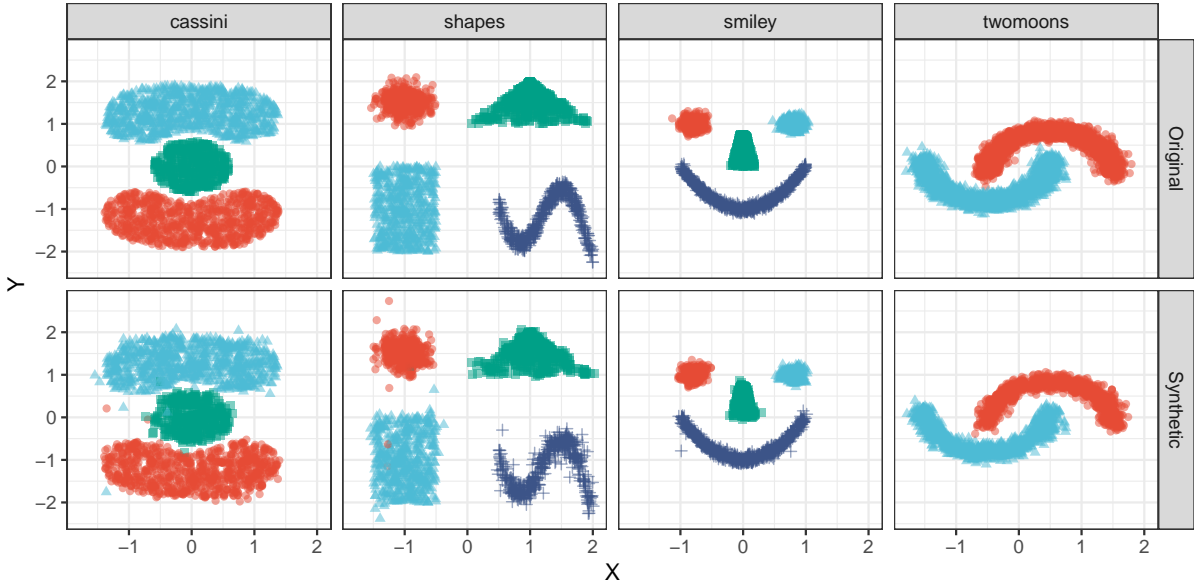


Figure 1: Visual examples. Original (top) and synthetic (bottom) data are presented for four three-dimensional problems with two continuous covariates and a single categorical feature.

FORGE outperforms alternative RF-based methods. We simulate data from a multivariate Gaussian distribution $\mathcal{N}(0, \Sigma)$, with Toeplitz covariance matrix $\Sigma_{ij} = 0.5^{|i-j|}$ and fixed $d = 10$. To compare against supervised methods, we also simulate a binary target $Y \sim \text{Bern}([1 + \exp(-\mathbf{X}\boldsymbol{\beta})]^{-1})$, where the coefficient vector $\boldsymbol{\beta}$ contains a varying proportion of 0’s (non-informative features) and 1’s (informative features). Parameters $\hat{\mu}$ and $\hat{\Sigma}$ are estimated from synthetic data via MLE. We record the Kullback–Leibler (KL) divergence between the ground truth distribution $\mathcal{N}(0, \Sigma)$ and the estimated $\mathcal{N}(\hat{\mu}, \hat{\Sigma})$. We compare our method to piecewise constant (PWC) estimators with supervised and unsupervised split criteria,² as well as generative forests (GeFs), a smooth conditional density estimation procedure [19].

Fig. 2 shows the average KL-divergence over 20 replicates for varying sample sizes (A) and levels of sparsity (B). For the former, we fix the proportion of informative features at 0.5; for the latter, we fix $n = 10,000$. We find that unsupervised methods dominate at all sample sizes, with the PWC variant performing well for small n before FORGE overtakes around $n = 1000$. We observe several interesting trends in the sparsity experiment, where PWC estimators appear to do worse with more informative features, while GeFs do best with very weak or very strong signals. This can be explained by the fact that splits are purely random when no features are informative, a strategy that is known to work well in noisy settings [35, 34]. Performance degrades as more informative features are added, since supervised models narrowly focus on these predictors to the exclusion of uninformative covariates, which comprise the majority of the data. Things reach a tipping point around 0.5, at which point most features provide signal and models gradually stabilize (PWC) or improve again (GeFs). Unsupervised split criteria, by contrast, show less variation in general and uniformly stronger performance in the case of FORGE.

5.2 Real Data

To evaluate the performance of FORGE on real-world datasets, we recreate a benchmarking pipeline originally proposed by Xu et al. [92]. They introduce the conditional tabular GAN (CTGAN) and tabular VAE (TVAE), two deep learning algorithms for generative modeling with mixed continuous and categorical features. It is straightforward to augment their benchmark with FORGED data to ensure adequate parameter configurations for deep learning competitors, and mitigate potential biases stemming from selective experimental designs.

A complete summary of the experimental setup is presented in Appx. B. Briefly, we take seven benchmark datasets for classification and partition the samples into training and test sets, which we

²Supervised PWC is simply an ensemble version of the classic method [38, 65, 91]. To the best of our knowledge, no one has previously proposed unsupervised PWC density estimation with CART trees. This can be understood as a variant of our approach in which all marginals are uniform within each leaf.

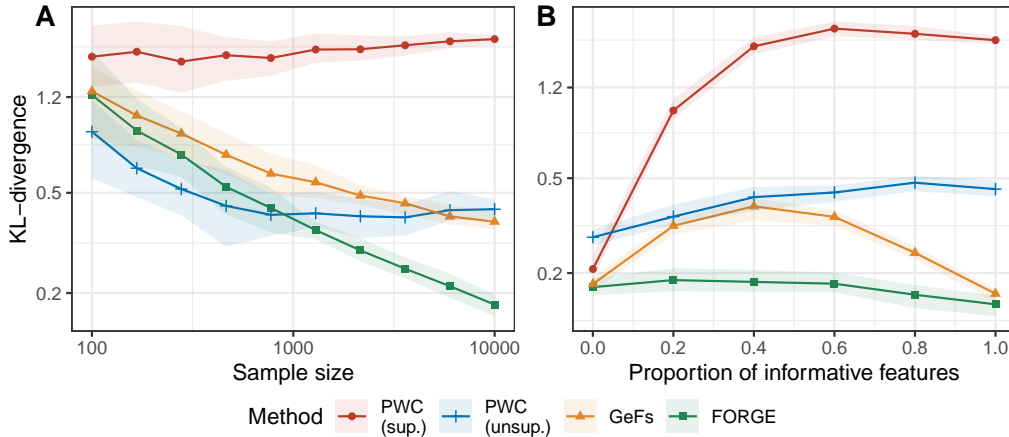


Figure 2: KL-divergence between ground truth and estimated distribution of data generated with PWC (supervised and unsupervised), GeFs, and FORGE for varying sample size (A) and sparsity (B).

denote by $\mathbf{Z}_{\text{trn}} = (\mathbf{X}_{\text{trn}}, Y_{\text{trn}})$ and $\mathbf{Z}_{\text{tst}} = (\mathbf{X}_{\text{tst}}, Y_{\text{tst}})$, respectively. \mathbf{Z}_{trn} is then used as input to a series of generative models, each of which creates a synthetic training set $\tilde{\mathbf{Z}}_{\text{trn}}$ of the same sample size as the original. Several classifiers are then trained on $\tilde{\mathbf{Z}}_{\text{trn}}$ and evaluated on \mathbf{Z}_{tst} , with performance metrics averaged across learners. Results are benchmarked against the same set of algorithms, now trained on the original data \mathbf{Z}_{trn} . We refer to this model as the *Oracle*, since it should perform no worse in expectation than any classifier trained on synthetic data. However, if the generative model has done a good job learning the true joint density, then differences between the Oracle and its competitors may be negligible. Similar approaches are widely used in the evaluation of GANs [93, 76, 72]; for a critical discussion, see [68].

Results are reported in Table 1, where we average over five trials of data synthesis and subsequent supervised learning. Performance is evaluated via accuracy and F1-score, as well as wall time. We find that FORGE is the most accurate method in five out of seven tasks, and has the highest F1-score in six out of seven. More impressive, it executes over 100 times faster than CTGAN and over 50 times faster than TVAE on average. Differences in compute time would be even more dramatic if these deep learning algorithms were configured with a CPU backend (we used GPUs here), or if FORGE were run using more extensive parallelization (we distribute the job across 10 cores). This comparison also obscures the extra time required to tune hyperparameters for these complex models, whereas our method is an off-the-shelf solution that works well with default settings.

5.3 Runtime

To further demonstrate the computational efficiency of our pipeline relative to deep learning methods, we conduct a runtime experiment using the smallest dataset above, `adult`. By repeatedly sampling stratified subsets—varying both sample size n and dimensionality d —and measuring the time needed to train a generative model and synthesize data from it, we illustrate how complexity scales with n and d . For this experiment, we ran CTGAN and TVAE with both CPU and GPU backends. We use default parameters for both algorithms, which include automated parallelization over all available cores (24 in this experiment). FORGE clearly dominates in all settings, with especially impressive performance in model training. For those with limited access to GPUs, deep learning methods may be completely infeasible for large datasets. Even when GPUs are available, FORGE still scales far better, executing the full pipeline about 35 times faster than TVAE and 85 times faster than CTGAN in this example. Note that FORGE also outperforms both in terms of accuracy and F1-score for the `adult` dataset, so the speedup need not come at the cost of performance.

6 Discussion

ARFs enable fast, accurate density estimation and data synthesis. However, the method is not without its limitations. First, it is not tailored to structured data such as images or text, for which deep learning models have proven especially effective. See Appx. B for a comparison to state of the art models for

Table 1: Average results across five replicates. We report regular F1-scores for binary classification tasks, and F1 macro-scores for multiclass problems (see Appx. B for details). The dimensionality d reported amongst other dataset characteristics excludes the target variable. Wall time is measured with GPU backends for CTGAN and TVAE, while FORGE is run in parallel on 10 CPU cores.

Dataset	Characteristics	Model	Accuracy (sd)	F1 (sd)	Time in sec
adult		<i>Oracle</i>	<i>0.828 (0.006)</i>	<i>0.884 (0.004)</i>	
	$n = 32,561$	FORGE	0.819 (0.006)	0.877 (0.005)	2.9
	$d = 14$	CTGAN	0.786 (0.020)	0.853 (0.019)	263.3
	classes = 2	TVAE	0.804 (0.007)	0.865 (0.006)	115.1
census		<i>Oracle</i>	<i>0.922 (0.002)</i>	<i>0.957 (0.001)</i>	
	$n = 298,006$	FORGE	0.903 (0.019)	0.946 (0.012)	53.2
	$d = 40$	CTGAN	0.916 (0.015)	0.954 (0.009)	4,287.8
	classes = 2	TVAE	0.928 (0.007)	0.961 (0.004)	1,814.9
coverttype		<i>Oracle</i>	<i>0.895 (0.000)</i>	<i>0.838 (0.000)</i>	
	$n = 581,012$	FORGE	0.707 (0.006)	0.549 (0.006)	103.5
	$d = 54$	CTGAN	0.633 (0.009)	0.400 (0.009)	13,387.2
	classes = 7	TVAE	0.698 (0.013)	0.459 (0.013)	4,882.0
credit		<i>Oracle</i>	<i>0.997 (0.001)</i>	<i>0.607 (0.029)</i>	
	$n = 284,807$	FORGE	0.995 (0.001)	0.527 (0.036)	32.2
	$d = 30$	CTGAN	0.881 (0.099)	0.047 (0.031)	4,898.0
	classes = 2	TVAE	0.998 (0.000)	0.000 (0.000)	3,847.6
intrusion		<i>Oracle</i>	<i>0.998 (0.001)</i>	<i>0.833 (0.001)</i>	
	$n = 494,021$	FORGE	0.993 (0.001)	0.656 (0.001)	68.2
	$d = 40$	CTGAN	0.944 (0.088)	0.645 (0.088)	8,749.3
	classes = 5	TVAE	0.990 (0.002)	0.598 (0.002)	4,306.0
mnist12		<i>Oracle</i>	<i>0.892 (0.003)</i>	<i>0.891 (0.003)</i>	
	$n = 70,000$	FORGE	0.799 (0.007)	0.795 (0.007)	32.5
	$d = 144$	CTGAN	0.172 (0.032)	0.138 (0.032)	2,737.4
	classes = 10	TVAE	0.763 (0.002)	0.761 (0.002)	1,143.8
mnist28		<i>Oracle</i>	<i>0.918 (0.002)</i>	<i>0.917 (0.002)</i>	
	$n = 70,000$	FORGE	0.729 (0.008)	0.723 (0.008)	169.5
	$d = 784$	CTGAN	0.197 (0.051)	0.167 (0.051)	14,415.4
	classes = 10	TVAE	0.698 (0.016)	0.697 (0.016)	5,056.0

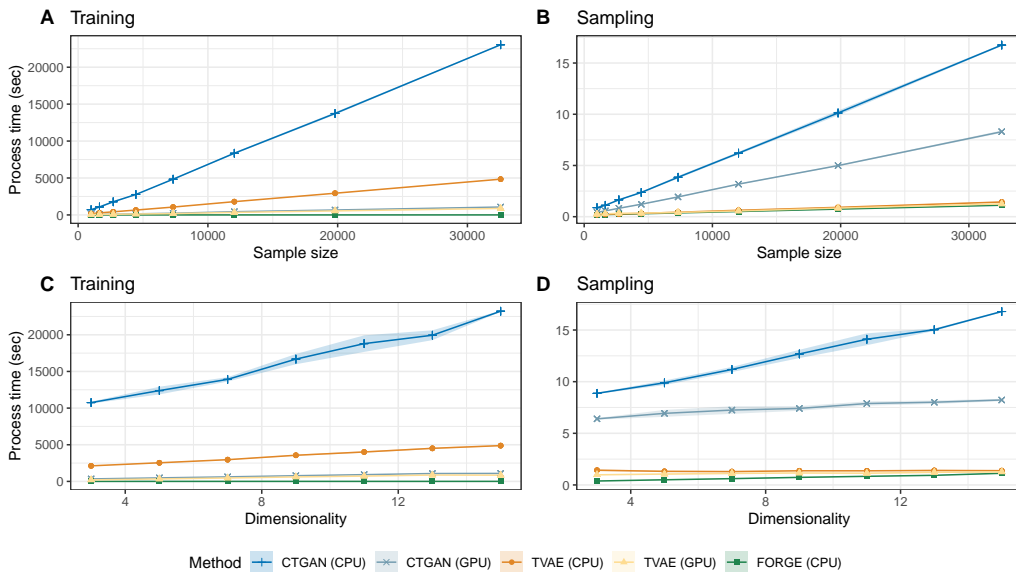


Figure 3: Complexity curves, evaluated using stratified subsamples of the **adult** dataset. **(A)**: Training time as a function of sample size. **(B)**: Sampling time as a function of sample size. **(C)**: Training time as a function of dimensionality. **(D)**: Sampling time as a function of dimensionality.

the `mnist28` dataset, where convolutional networks clearly outperform FORDE and FORGE, as expected. Where our method excels, by contrast, is in speed and flexibility.

One potential difficulty for our approach is selecting an optimal density estimation subroutine. KDE relies on a smoothness assumption (A4), while MLE requires a (local) parametric model. Both methods will struggle when their assumptions are violated. Resampling alternatives such as permutations or bootstrapping do not produce any data that was not observed in the training set and may therefore raise privacy concerns. No method is generally guaranteed to strike the optimal balance between efficiency, accuracy, and privacy, and so the choice of which estimation procedure to employ for specific variables is irreducibly context-dependent.

We emphasize that our method performs well in a range of settings without any model tuning. However, we acknowledge that optimal performance likely depends on RF parameters [73, 63]. In particular, there is an inherent trade-off between the goals of minimizing errors of density (ϵ_2) and errors of convergence (ϵ_3) in finite samples. Grow trees too deep, and leaves will not contain enough data to accurately estimate marginal densities; grow trees too shallow, and ARFs may not satisfy the local independence criterion. Meanwhile, the `mtry` parameter has been shown to control sparsity in low signal-to-noise regimes [56]. Smaller values may therefore be appropriate when ϵ_3 is large, in order to regularize the forest. Adding more trees can stabilize results, though this incurs extra computational cost in both time and memory [62]. Despite these considerations, we reiterate that RFs are known to do well with default parameters, a trait that ARFs appear to inherit, judging by our experiments.

The ethical implications of generative models are potentially fraught. Deepfakes have attracted particular attention in this regard [25, 58, 22], as they can deceive their audience into believing that people said or did things they never in fact said or did. These dangers are most acute with convolutional neural networks or other architectures optimized for visual and audio data. Despite and in full awareness of these concerns, we highlight an ethical opportunity presented by FORGE, which can preserve the privacy of data subjects by creating datasets that capture all relevant signals without exposing the personal information of any individual. This is especially valuable in sensitive areas like healthcare and finance, where data breaches are common and potentially disastrous. As with all powerful technologies, caution is advised and regulatory frameworks are welcome.

7 Conclusion

We have introduced a novel procedure for learning joint densities and generating synthetic data using a recursive, adversarial variant of unsupervised random forests. The method is provably consistent under reasonable assumptions, and performs well in experiments on simulated and real-world examples. Our FORDE algorithm is more accurate than leading tree-based alternatives, and more scalable than methods that require multivariate density estimation. Our FORGE algorithm is competitive with state of the art deep learning models for data generation on tabular benchmarks, and routinely executes some 100 times faster.

Future work will explore further applications for these methods, such as outlier detection, clustering, and classification, as well as potential connections with differential privacy [27]. Alternative tree-based solutions based on gradient boosting also warrant further exploration, especially given some promising recent developments in this area [31, 33].

References

- [1] Nelson Lee Afanador, Agnieszka Smolinska, Thanh N. Tran, and Lionel Blanchet. Unsupervised random forest: a tutorial with case studies. *J. Chemom.*, 30(5):232–241, 2016.
- [2] Martin Arjovsky, Soumith Chintala, and Léon Bottou. Wasserstein generative adversarial networks. In *Proceedings of the 34th International Conference on Machine Learning*, page 214–223, 2017.
- [3] Susan Athey, Julie Tibshirani, and Stefan Wager. Generalized random forests. *Ann. Statist.*, 47(2): 1148–1178, 2019.
- [4] Sean Augenstein, H. Brendan McMahan, Daniel Ramage, Swaroop Ramaswamy, Peter Kairouz, Mingqing Chen, Rajiv Mathews, and Blaise Agüera y Arcas. Generative models for effective ML on private, decentralized datasets. In *International Conference on Learning Representations*, 2020.

- [5] Francis R. Bach and Michael I. Jordan. Beyond independent components: Trees and clusters. *J. Mach. Learn. Res.*, 4:1205–1233, 2003.
- [6] Mariana Belgiu and Lucian Drăguț. Random forest in remote sensing: A review of applications and future directions. *ISPRS J. Photogramm. Remote Sens.*, 114:24–31, 2016.
- [7] Gérard Biau. Analysis of a random forests model. *J. Mach. Learn. Res.*, 13:1063–1095, 2012.
- [8] Gérard Biau, Luc Devroye, and Gábor Lugosi. Consistency of random forests and other averaging classifiers. *J. Mach. Learn. Res.*, 9(66):2015–2033, 2008.
- [9] Gérard Biau and Luc Devroye. On the layered nearest neighbour estimate, the bagged nearest neighbour estimate and the random forest method in regression and classification. *J. Multivar. Anal.*, 101(10):2499–2518, 2010.
- [10] Jock A. Blackard. Covertypes data set, 1999. URL <https://archive.ics.uci.edu/ml/datasets/covertypes>.
- [11] Max Bramer. *Clustering*, pages 221–238. Springer, London, UK, 2007.
- [12] Leo Breiman. Random forests. *Mach. Learn.*, 45(1):1–33, 2001.
- [13] Leo Breiman. Consistency for a simple model of random forests. Technical Report 670, Statistics Department, UC Berkeley, Berkeley, CA, 2004.
- [14] Leo Breiman, Jerome Friedman, C. J. Stone, and R. A. Olshen. *Classification and Regression Trees*. Taylor & Francis, Boca Raton, FL, 1984.
- [15] Igor Buzhinsky, Arseny Nerinovsky, and Stavros Tripakis. Metrics and methods for robustness evaluation of neural networks with generative models. *Mach. Learn.*, 2021.
- [16] Varun Chandola, Arindam Banerjee, and Vipin Kumar. Anomaly detection: A survey. *ACM Comput. Surv.*, 41(3), 2009.
- [17] Xi Chen and Hemant Ishwaran. Random forests for genomic data analysis. *Genomics*, 99(6):323–329, 2012.
- [18] Edward Choi, Siddharth Biswal, Bradley Malin, Jon Duke, Walter F. Stewart, and Jimeng Sun. Generating multi-label discrete patient records using generative adversarial networks. In *Proceedings of the 2nd Machine Learning for Healthcare Conference*, volume 68 of *Proceedings of Machine Learning Research*, pages 286–305, 2017.
- [19] Alvaro Correia, Robert Peharz, and Cassio P de Campos. Joints in random forests. In *Advances in Neural Information Processing Systems*, volume 33, pages 11404–11415, 2020.
- [20] Antonio Criminisi, Jamie Shotton, and Ender Konukoglu. *Decision Forests: A Unified Framework for Classification, Regression, Density Estimation, Manifold Learning and Semi-Supervised Learning*, volume 7, pages 81–227. NOW Publishers, Norwell, MA, 2012.
- [21] D. Richard Cutler, Thomas C. Edwards Jr., Karen H. Beard, Adele Cutler, Kyle T. Hess, Jacob Gibson, and Joshua J. Lawler. Random forests for classification in ecology. *Ecology*, 88(11):2783–2792, 2007.
- [22] Adrienne de Ruyter. The distinct wrong of deepfakes. *Philos. Technol.*, 34(4):1311–1332, 2021.
- [23] Misha Denil, David Matheson, and Nando De Freitas. Narrowing the gap: Random forests in theory and in practice. In *Proceedings of the 31st International Conference on Machine Learning*, pages 665–673, 2014.
- [24] Luc Devroye, László Györfi, and Gábor Lugosi. *A Probabilistic Theory of Pattern Recognition*. Springer-Verlag, New York, 1996.
- [25] Nicholas Diakopoulos and Deborah Johnson. Anticipating and addressing the ethical implications of deepfakes in the context of elections. *New Media Soc.*, 23(7):2072–2098, 2021.

- [26] Dheeru Dua and Casey Graff. UCI machine learning repository, 2019. URL <http://archive.ics.uci.edu/ml>.
- [27] Cynthia Dwork. Differential privacy: A survey of results. In *Theory and Applications of Models of Computation*, volume 4978, pages 1–19, Berlin, Heidelberg, 2008. Springer.
- [28] Bradley Efron. Missing data, imputation, and the bootstrap. *J. Am. Stat. Assoc.*, 89(426):463–475, 1994.
- [29] Ji Feng and Zhi-Hua Zhou. Autoencoder by forest. In *Proceedings of the 32nd AAAI Conference on Artificial Intelligence*, 2018.
- [30] Manuel Fernández-Delgado, Eva Cernadas, Senén Barro, and Dinani Amorim. Do we need hundreds of classifiers to solve real world classification problems? *J. Mach. Learn. Res.*, 15(90):3133–3181, 2014.
- [31] Jerome H. Friedman. Contrast trees and distribution boosting. *Proc. Natl. Acad. Sci.*, 117(35):21175–21184, 2020.
- [32] Wei Gao and Zhi-Hua Zhou. Towards convergence rate analysis of random forests for classification. In *Advances in Neural Information Processing Systems*, volume 33, pages 9300–9311, 2020.
- [33] Zijun Gao and Trevor Hastie. LinCDE: Conditional density estimation via Lindsey’s method. *J. Mach. Learn. Res.*, 23(52):1–55, 2022.
- [34] Robin Genuer. Variance reduction in purely random forests. *J. Nonparametr. Stat.*, 24(3):543–562, 2012.
- [35] Pierre Geurts, Damien Ernst, and Louis Wehenkel. Extremely randomized trees. *Mach. Learn.*, 63(1):3–42, 2006.
- [36] Ian J. Goodfellow, Jean Pouget-Abadie, Mehdi Mirza, Bing Xu, David Warde-Farley, Sherjil Ozair, Aaron Courville, and Yoshua Bengio. Generative adversarial nets. In *Advances in Neural Information Processing Systems*, volume 27, page 2672–2680, 2014.
- [37] Artur Gramacki. *Nonparametric Kernel Density Estimation and Its Computational Aspects*. Springer, Cham, 2018.
- [38] Alexander G. Gray and Andrew W. Moore. Nonparametric density estimation: Toward computational tractability. In *Proceedings of the 2003 SIAM International Conference on Data Mining (SDM)*, pages 203–211, 2003.
- [39] Irina Higgins, Loïc Matthey, Arka Pal, Christopher Burgess, Xavier Glorot, Matthew Botvinick, Shakir Mohamed, and Alexander Lerchner. β -VAE: Learning basic visual concepts with a constrained variational framework. In *International Conference on Learning Representations*, 2017.
- [40] James Jordon, Jinsung Yoon, and Mihaela van der Schaar. PATE-GAN: generating synthetic data with differential privacy guarantees. In *International Conference on Learning Representations*, 2019.
- [41] Ilmun Kim, Aaditya Ramdas, Aarti Singh, and Larry Wasserman. Classification accuracy as a proxy for two-sample testing. *Ann. Stat.*, 49(1):411 – 434, 2021.
- [42] Diederik Kingma and Max Welling. Auto-encoding variational Bayes. In *International Conference on Learning Representations*, 2013.
- [43] Diederik Kingma, Tim Salimans, Ben Poole, and Jonathan Ho. Variational diffusion models. In *Advances in Neural Information Processing Systems*, volume 34, pages 21696–21707, 2021.
- [44] Ivan Kobyzev, Simon J.D. Prince, and Marcus A. Brubaker. Normalizing flows: An introduction and review of current methods. *IEEE Transactions on Pattern Analysis and Machine Intelligence*, 43(11):3964–3979, 2021.
- [45] Yann LeCun, Léon Bottou, Yoshua Bengio, and Patrick Haffner. Gradient-based learning applied to document recognition. *Proceedings of the IEEE*, 86(11):2278–2324, 1998.

- [46] Jaewoo Lee, Minjung Kim, Yonghyun Jeong, and Youngmin Ro. Differentially private normalizing flows for synthetic tabular data generation. *Proceedings of the AAAI Conference on Artificial Intelligence*, 36(7):7345–7353, 2022.
- [47] Han Liu, Min Xu, Haijie Gu, Anupam Gupta, John Lafferty, and Larry Wasserman. Forest density estimation. *J. Mach. Learn. Res.*, 12(25):907–951, 2011.
- [48] Wei-Yin Loh. Improving the precision of classification trees. *Ann. Appl. Stat.*, 3(4):1710 – 1737, 2009.
- [49] Romain Lopez, Jeffrey Regier, Michael B Cole, Michael I Jordan, and Nir Yosef. Deep generative modeling for single-cell transcriptomics. *Nat. Methods*, 15(12):1053–1058, 2018. ISSN 1548-7105.
- [50] Gábor Lugosi and Andrew Nobel. Consistency of data-driven histogram methods for density estimation and classification. *Ann. Stat.*, 24(2):687 – 706, 1996.
- [51] Scott M Lundberg, Gabriel Erion, Hugh Chen, Alex DeGrave, Jordan M Prutkin, Bala Nair, Ronit Katz, Jonathan Himmelfarb, Nisha Bansal, and Su-In Lee. From local explanations to global understanding with explainable AI for trees. *Nat. Mach. Intell.*, 2(1):56–67, 2020.
- [52] J.D. Malley, J. Kruppa, A. Dasgupta, K.G. Malley, and A. Ziegler. Probability Machines: Consistent probability estimation using nonparametric learning machines. *Methods Inf. Med.*, 51(1):74–81, 2012.
- [53] Alejandro Mantero and Hemant Ishwaran. Unsupervised random forests. *Stat. Anal. Data. Min.*, 14(2):144–167, 2021.
- [54] Nicolai Meinshausen. Quantile regression forests. *J. Mach. Learn. Res.*, 7:983–999, 2006.
- [55] Lucas Mentch and Giles Hooker. Quantifying uncertainty in random forests via confidence intervals and hypothesis tests. *J. Mach. Learn. Res.*, 17(26), 2016.
- [56] Lucas Mentch and Siyu Zhou. Randomization as regularization: A degrees of freedom explanation for random forest success. *J Mach. Learn. Res.*, 21(171), 2020.
- [57] Mehdi Mirza and Simon Osindero. Conditional generative adversarial nets. *arXiv preprint*, 1411.1784, 2014.
- [58] Carl Öhman. Introducing the pervert’s dilemma: a contribution to the critique of deepfake pornography. *Ethics Inf. Technol.*, 22(2):133–140, 2020.
- [59] Guansong Pang, Chunhua Shen, Longbing Cao, and Anton Van Den Hengel. Deep learning for anomaly detection: A review. *ACM Comput. Surv.*, 54(2), 2021.
- [60] George Papamakarios, Eric Nalisnick, Danilo Jimenez Rezende, Shakir Mohamed, and Balaji Lakshminarayanan. Normalizing flows for probabilistic modeling and inference. *J. Mach. Learn. Res.*, 22(57):1–64, 2021.
- [61] Wei Peng, Tim Coleman, and Lucas Mentch. Rates of convergence for random forests via generalized U-statistics. *Electron. J. Stat.*, 16(1):232 – 292, 2022.
- [62] Philipp Probst and Anne-Laure Boulesteix. To tune or not to tune the number of trees in random forest. *J. Mach. Learn. Res.*, 18(1):6673–6690, 2017.
- [63] Philipp Probst, Marvin N. Wright, and Anne-Laure Boulesteix. Hyperparameters and tuning strategies for random forest. *WIREs Data Mining and Knowledge Discovery*, 9(3):e1301, 2019.
- [64] Tahrima Rahman, Prasanna Kothalkar, and Vibhav Gogate. Cutset networks: A simple, tractable, and scalable approach for improving the accuracy of Chow-Liu trees. In *Machine Learning and Knowledge Discovery in Databases*, pages 630–645, Berlin, Heidelberg, 2014. Springer Berlin Heidelberg.
- [65] Parikshit Ram and Alexander G. Gray. Density estimation trees. In *Proceedings of the 17th ACM SIGKDD International Conference on Knowledge Discovery and Data Mining*, page 627–635, 2011.
- [66] Aditya Ramesh, Mikhail Pavlov, Gabriel Goh, Scott Gray, Chelsea Voss, Alec Radford, Mark Chen, and Ilya Sutskever. Zero-shot text-to-image generation. *arXiv preprint*, 2102.12092, 2021.

- [67] Aditya Ramesh, Prafulla Dhariwal, Alex Nichol, Casey Chu, and Mark Chen. Hierarchical text-conditional image generation with CLIP latents. *arXiv preprint*, 2204.06125, 2022.
- [68] Suman Ravuri and Oriol Vinyals. Classification accuracy score for conditional generative models. In *Advances in Neural Information Processing Systems*, volume 32, 2019.
- [69] Lior Rokach and Oded Maimon. *Clustering Methods*, pages 321–352. Springer US, Boston, MA, 2005.
- [70] Aurko Roy, Mohammad Saffar, Ashish Vaswani, and David Grangier. Efficient content-based sparse attention with routing transformers. *Transactions of the Association for Computational Linguistics*, 9:53–68, 2021.
- [71] Donald B. Rubin. Multiple imputation after 18+ years. *J. Am. Stat. Assoc.*, 91(434):473–489, 1996.
- [72] Shibani Santurkar, Ludwig Schmidt, and Aleksander Madry. A classification-based study of covariate shift in GAN distributions. In *Proceedings of the 35th International Conference on Machine Learning*, volume 80, pages 4480–4489, 2018.
- [73] Erwan Scornet. Tuning parameters in random forests. *ESAIM: Procs*, 60:144–162, 2017.
- [74] Erwan Scornet, Gerard Biau, and Jean Philippe Vert. Consistency of random forests. *Ann. Statist.*, 43(4):1716–1741, 2015.
- [75] Tao Shi and Steve Horvath. Unsupervised learning with random forest predictors. *J. Comput. Graph. Stat.*, 15(1):118–138, 2006.
- [76] Konstantin Shmelkov, Cordelia Schmid, and Karteek Alahari. How good is my GAN? In *Computer Vision – ECCV 2018*, pages 218–234, Cham, 2018. Springer International Publishing.
- [77] Bernard Silverman. *Density Estimation for Statistics and Data Analysis*. Chapman & Hall, London, 1986.
- [78] Padhraic Smyth, Alexander G. Gray, and Usama M. Fayyad. Retrofitting decision tree classifiers using kernel density estimation. In *Proceedings of the 12th International Conference on International Conference on Machine Learning*, page 506–514, 1995.
- [79] Yang Song, Rui Shu, Nate Kushman, and Stefano Ermon. Constructing unrestricted adversarial examples with generative models. In *Advances in Neural Information Processing Systems*, volume 31, 2018.
- [80] Yang Song, Jascha Sohl-Dickstein, Diederik Kingma, Abhishek Kumar, Stefano Erman, and Ben Poole. Score-based generative modeling through stochastic differential equations. In *International Conference on Learning Representations*, 2021.
- [81] Daniel J Stekhoven and Peter Bühlmann. MissForest—non-parametric missing value imputation for mixed-type data. *Bioinformatics*, 28(1):112–118, 2011.
- [82] Fei Tang and Hemant Ishwaran. Random forest missing data algorithms. *Stat. Anal. Data Min.*, 10(6):363–377, 2017.
- [83] Aäron van den Oord, Nal Kalchbrenner, and Koray Kavukcuoglu. Pixel recurrent neural networks. In *Proceedings of The 33rd International Conference on Machine Learning*, volume 48, pages 1747–1756, 2016.
- [84] V. N. Vapnik and A. Ya. Chervonenkis. *On the Uniform Convergence of Relative Frequencies of Events to Their Probabilities*, pages 11–30. Springer International Publishing, Cham, 2015.
- [85] Pascal Vincent and Yoshua Bengio. Manifold Parzen windows. In *Advances in Neural Information Processing Systems*, volume 15, 2002.
- [86] Stefan Wager and Susan Athey. Estimation and inference of heterogeneous treatment effects using random forests. *J. Am. Stat. Assoc.*, 113(523):1228–1242, 2018.
- [87] Stefan Wager and Walther Guenther. Adaptive concentration of regression trees, with application to random forests. *arXiv preprint*, 1503.06388, 2015.

- [88] M.P. Wand and M.C. Jones. *Kernel Smoothing*. Chapman & Hall, Boca Raton, FL, 1994.
- [89] Hongwei Wen and Hanyuan Hang. Random forest density estimation. In *Proceedings of the 39th International Conference on Machine Learning*, pages 23701–23722, 2022.
- [90] Worldline and the ML Group of ULB. Credit card fraud detection data. license: Open database., 2013. URL <https://www.kaggle.com/datasets/mlg-ulb/creditcardfraud>.
- [91] Ke Wu, Kun Zhang, Wei Fan, Andrea Edwards, and Philip S. Yu. RS-Forest: A rapid density estimator for streaming anomaly detection. In *2014 IEEE International Conference on Data Mining*, pages 600–609, 2014.
- [92] Lei Xu, Maria Skoularidou, Alfredo Cuesta-Infante, and Kalyan Veeramachaneni. Modeling tabular data using conditional GAN. In *Advances in Neural Information Processing Systems*, volume 32, 2019.
- [93] Jianwei Yang, Anitha Kannan, Dhruv Batra, and Devi Parikh. LR-GAN: Layered recursive generative adversarial networks for image generation. In *International Conference on Learning Representations*, 2017.
- [94] Burak Yelmen, Aurélien Decelle, Linda Ongaro, Davide Marnetto, Coentin Tallec, Francesco Montinaro, Cyril Furtlehner, Luca Pagani, and Flora Jay. Creating artificial human genomes using generative neural networks. *PLOS Genetics*, 17(2):1–22, 02 2021.

A Proofs

A.1 Proof of Thm. 1

To secure the result, we must show that (a) the discriminator reliably converges on the Bayes risk at each iteration t ; and (b) the generator’s sampling strategy drives original and synthetic data closer together, ultimately driving the Bayes risk to $1/2$ as $n, t \rightarrow \infty$. (For the purposes of this proof, we set the tolerance parameter δ to 0.)

Take (a) first. This amounts to a consistency requirement for RFs. The consistency of RF classifiers has been shown under various assumptions about splitting rules and stopping criteria [13, 8, 9], but these results generally require trees to be grown to purity or even completion (i.e., $n_b^\ell = 1$ for all ℓ, b). However, this would turn the generator’s sampling strategy into a simple copy-paste operation and make intra-leaf density estimation impossible. We therefore follow Malley et al. [52] in observing that regression procedures constitute probability machines, since $P(Y = 1|\mathbf{x}) = \mathbb{E}[Y|\mathbf{x}]$ for $Y \in \{0, 1\}$.

The honesty and regularity conditions originally introduced by Wager and Athey [86]—subsequently generalized by Athey et al. [3] and further studied by Peng et al. [61]—are well-suited to our task. They provide consistency criteria for regression forests that apply to RF classifiers as a special case when predictions are made via soft labeling. For full details, we refer readers to the original texts. We simply summarize the most pertinent results below, which involve the bias-variance decomposition of RF predictions. Under (A1)-(A3), bias decays at the following rate [86, Thm. 3.2]:

$$|\mathbb{E}[f(\mathbf{x})] - \mathbb{E}[Y|\mathbf{x}]| = \mathcal{O}\left(n_b^{-\frac{1}{2} \frac{\log((1-\gamma)^{-1})}{\log(\gamma^{-1})} \frac{\pi}{d}}\right).$$

Meanwhile, variance decays according to Wager and Athey [86, Appx. C.2]:

$$\mathbb{E}\left[\left[f(\mathbf{x}) - \mathbb{E}[f(\mathbf{x})]\right]^2\right] = \mathcal{O}\left(n_b^{-\frac{\log((1-\gamma)^{-1})}{\log(\gamma^{-1})} \frac{\pi}{d}}\right).$$

Since L_2 error is just the sum of squared bias, variance, and irreducible error terms, any RF classifier satisfying (A1)-(A3) will converge as n grows large.³

Desideratum (b) effectively says that original and synthetic data become indistinguishable as n and t increase. For simplicity, we focus on the single tree case. (The consistency of the ensemble follows from the consistency of the base method [8].) In the asymptotic regime, we need some stopping criterion to trigger potential recursion, or else we are indefinitely stuck on $t = 0$. Let $\text{diam}(\ell)$ denote the diameter of leaf ℓ , i.e. the length of the longest segment contained in \mathcal{X}^ℓ . Meinshausen [54, Lemma 2] shows that under the regularity conditions of (A3), $\text{diam}(\ell) \rightarrow_p 0$ for all ℓ as $n \rightarrow \infty$. For the purposes of this proof, we consider a modified version of the algorithm in which the maximum permissible leaf diameter decreases as a function of t . That is, for all $t \in \mathbb{N}$ and some $v \in [0, 1]$, we grow $f^{(t)}$ until $\max_\ell (\text{diam}(\ell)) \leq v/(t+1)$.

At $t = 0$, we generate synthetic data $\mathbf{x}^{(0)} \sim \prod_{j=1}^d P(X_j)$, which becomes input to the discriminator $f^{(0)}$. Let θ_0 denote the resulting splits once our stopping criterion is met. We then sample leaves according to their coverage $\ell \sim q(\theta_0^\ell)$, and generate new data $\mathbf{x}^{(1)} \sim \prod_{j=1}^d P(X_j|\theta_0^\ell)$, which in turn becomes input to the discriminator $f^{(1)}$. This sampling strategy tends to down-weight low-density regions and concentrate in high-density regions. (The consistency of coverage estimates is treated separately in Appx. A.3.) Leaves with relatively little real data are pruned, as new synthetic data is sampled from leaves that overlap more closely with the true data manifold. As the synthetic data draws closer to the original with each passing round, the maximum leaf diameter shrinks, creating leaves of increasing density. This results in an infinitesimally small bounding box in which to sample synthetic data. Since these points are arbitrarily close to their original counterparts from the same leaf, the two classes cannot be reliably distinguished and Bayes risk converges to $1/2$.

³Strictly speaking, the honesty condition (i) is not necessary to prove the consistency of RFs. However, it does tend to reduce bias, especially in the presence of outliers, and guarantees asymptotic normality of RF predictions. Alternative consistency conditions for adaptive split trees require either further assumptions about the data generating process [74] or modifications to the algorithm itself [87]. See Wager and Athey [86, Appx. B] for a discussion.

A.2 Proof of Lemma 1

Define the first-order approximation to p satisfying local independence:

$$\hat{p}(\mathbf{x}) = \frac{1}{B} \sum_{\ell, b: \mathbf{x} \in \mathcal{X}_b^\ell} p(\theta_b^\ell) \prod_{j=1}^d p(x_j | \theta_b^\ell).$$

We also define the root integrated squared error (RISE), i.e. the Euclidean distance between probability densities:

$$\text{RISE}(p, q) := \left(\int_{\mathcal{X}} (p(\mathbf{x}) - q(\mathbf{x}))^2 d\mathbf{x} \right)^{1/2}.$$

By the triangle inequality, we have:

$$\text{RISE}(p, q) \leq \text{RISE}(p, \hat{p}) + \text{RISE}(\hat{p}, q).$$

Squaring both sides, we get:

$$\text{ISE}(p, q) \leq \text{ISE}(p, \hat{p}) + \text{ISE}(\hat{p}, q) + 2 \text{RISE}(p, \hat{p}) \text{RISE}(\hat{p}, q).$$

Adding a nonnegative constant to the rhs, we can reduce the expression:

$$\begin{aligned} \text{ISE}(p, q) &\leq \text{ISE}(p, \hat{p}) + \text{ISE}(\hat{p}, q) + 2 \text{RISE}(p, \hat{p}) \text{RISE}(\hat{p}, q) + (\text{RISE}(p, \hat{p}) - \text{RISE}(\hat{p}, q))^2 \\ &= 2(\text{ISE}(p, \hat{p}) + \text{ISE}(\hat{p}, q)). \end{aligned}$$

Now observe that we can rewrite both ISE formulae in terms of our predefined residuals (Eqs. 3-5):

$$\begin{aligned} \text{ISE}(p, \hat{p}) &= \int_{\mathcal{X}} \left(\frac{1}{B} \sum_{\ell, b: \mathbf{x} \in \mathcal{X}_b^\ell} (p(\theta_b^\ell) p(\mathbf{x} | \theta_b^\ell) - p(\theta_b^\ell) \prod_{j=1}^d p(x_j | \theta_b^\ell)) \right)^2 d\mathbf{x} \\ &= \frac{1}{B^2} \int_{\mathcal{X}} \left(\sum_{\ell, b: \mathbf{x} \in \mathcal{X}_b^\ell} p(\theta_b^\ell) \epsilon_3 \right)^2 d\mathbf{x}. \\ \text{ISE}(\hat{p}, q) &= \int_{\mathcal{X}} \left(\frac{1}{B} \sum_{\ell, b: \mathbf{x} \in \mathcal{X}_b^\ell} (p(\theta_b^\ell) \prod_{j=1}^d p(x_j | \theta_b^\ell) - q(\theta_b^\ell) \prod_{j=1}^d q(x_j; \theta_{b,j}^\ell)) \right)^2 d\mathbf{x} \\ &= \frac{1}{B^2} \int_{\mathcal{X}} \left(\sum_{\ell, b: \mathbf{x} \in \mathcal{X}_b^\ell} (p(\theta_b^\ell) \epsilon_2 + \epsilon_1 \prod_{j=1}^d p(x_j | \theta_b^\ell) - \epsilon_1 \epsilon_2) \right)^2 d\mathbf{x}. \end{aligned}$$

We replace the interior squared terms for ease of presentation:

$$\begin{aligned} \alpha &:= \sum_{\ell, b: \mathbf{x} \in \mathcal{X}_b^\ell} p(\theta_b^\ell) \epsilon_3 \\ \beta &:= \sum_{\ell, b: \mathbf{x} \in \mathcal{X}_b^\ell} (p(\theta_b^\ell) \epsilon_2 + \epsilon_1 \prod_{j=1}^d p(x_j | \theta_b^\ell) - \epsilon_1 \epsilon_2). \end{aligned}$$

Finally, we take expectations on both sides:

$$\text{MISE}(p, q) \leq 2B^{-2} \mathbb{E} \left[\int_{\mathcal{X}} \alpha^2 + \beta^2 d\mathbf{x} \right],$$

where we have exploited the linearity of expectation to pull the factor outside of the bracketed term, and the monotonicity of expectation to preserve the inequality.

A.3 Proof of Theorem 2

Lemma 1 states that error is bounded by a quadratic function of $\epsilon_1, \epsilon_2, \epsilon_3$. Thus for L_2 -consistency, it suffices to show that $\mathbb{E}[\epsilon_j^2] \rightarrow 0$, for $j \in \{1, 2, 3\}$. Since this is already established by Thm. 1 for $j = 3$, we focus here on errors of coverage and density. Start with ϵ_1 . A general version of the Glivenko-Cantelli

theorem [84] guarantees uniform convergence of empirical proportions to population proportions. Let \mathcal{L} denote the set of all possible hyperrectangular subspaces induced by axis-aligned splits on \mathcal{X} . Then we have that $\lim_{n \rightarrow \infty} \sup_{\ell \in \mathcal{L}} |p(\theta^\ell) - q(\theta^\ell)| = 0$ with probability 1.

Next, take ϵ_2 . (A5) guarantees that p satisfies the consistency conditions for univariate KDE [77, 88, 37], while condition (v) of (A4), originally due to Meinshausen [54], ensures that within-leaf sample size increases even as leaf volume goes to zero. Our kernel is a nonnegative function $K : \mathbb{R}^d \rightarrow \mathbb{R}$ that integrates to 1, parametrized by the bandwidth h :

$$p_h(\mathbf{x}) = \frac{1}{nh} \sum_{i=1}^n K\left(\frac{\mathbf{x} - \mathbf{x}_i}{h}\right).$$

Using standard arguments, we take a Taylor series expansion of the MISE and minimize the *asymptotic* MISE (AMISE):

$$\text{AMISE}(p, p_h) = \frac{1}{nh} R(K) + \frac{1}{4} h^4 \mu_2(K)^2 R(p''),$$

where

$$\begin{aligned} R(K) &= \int K(x)^2 dx, \\ \mu_2(K) &= \int x^2 K(x) dx, \text{ and} \\ R(p'') &= \int p''(x)^2 dx. \end{aligned}$$

For example values of these variables under specific kernels, see [88, Appx. B]. Under (A4), it can be shown that

$$\text{MISE}(p, p_h) = \text{AMISE}(p, p_h) + o((nh)^{-1} + h^4).$$

Thus if $(nh)^{-1} \rightarrow 0$ and $h \rightarrow 0$ as $n \rightarrow \infty$, the asymptotic approximation is exact and $\mathbb{E}[\epsilon_2^2] \rightarrow 0$.

These results, combined with the proof of Thm. 1 (see Appx. A.1), establish that errors of coverage, density, and convergence all vanish in the limit. Thus $\mathbb{E}[\epsilon_j^2] \rightarrow 0$ almost surely for $j \in \{1, 2, 3\}$, and the proof is complete.

B Experiments

Our experiments do not include any personal data, as defined in Article 4(1) of the European Union’s General Data Protection Regulation. All data are either simulated or from publicly available resources such as the University of California Irvine Machine Learning repository [26].

We performed all experiments on a dedicated 64-bit Linux platform running Ubuntu 20.04 with an AMD Ryzen Threadripper 3960X (24 cores, 48 threads) CPU, 256 gigabyte RAM and two NVIDIA Titan RTX GPUs. We used R version 4.1.2 and Python version 3.7.12. Further details on the environment setup are provided in the supplemental code.

B.1 Simulations

The `cassini`, `shapes`, and `smiley` simulations are all available in the `mlbench` R package; the `twomoons` problem is available in the `fdm2id` R package. Default parameters were used throughout, with fixed sample size $n = 2000$.

B.2 Real Data

For benchmarking generative models on real-world data, we use the benchmarking pipeline proposed by Xu et al. [92]. In detail, the workflow is as follows:

1. Load classification datasets used in Xu et al. [92], namely `adult`, `census`, `credit`, `covertype`, `intrusion`, `mnist12`, and `mnist28`. Note that the type of prediction task does not affect the process of synthetic data generation, so we omit the single regression example (`news`) for greater consistency.
2. Split the data into training and test sets (see Table 2 for details).

- Train the generative models FORGE (number of trees = 10, minimum node size = 5), CTGAN⁴ (batch size = 500, epochs = 300) and TVAE⁵ (batch size = 500, epochs = 300).
- Generate a synthetic dataset of the same size as the training set using each of the generative models trained in step (3), measuring the wall time needed to execute this task.
- Train a set of supervised learning algorithms (see Table 2 for details): (a) on the real training data set (i.e., the *Oracle*); and (b) on the synthetic training datasets generated by FORGE, CTGAN and TVAE.
- Evaluate the performance of the learning algorithms from step (5) on the test set.
- For each dataset, average performance metrics (accuracy, F1-scores) across learners. We report F1-scores for the positive class, e.g. '>50k' for *adult*, '+50000' for *census* and '1' for *credit*.

Table 2: Benchmark Setup. Supervised learning algorithms for prediction: (A) Adaboost, estimators = 50, (B) Decision Tree, tree depth for binary/multiclass target = 15/30, (C) Logistic Regression, (D) MLP, hidden layers for binary/multiclass target = 50/100

Dataset	Train/Test Set	Learner	Link to dataset
<i>adult</i> [26]	23k/10k	A,B,C,D	http://archive.ics.uci.edu/ml/datasets/adult
<i>census</i> [26]	200k/100k	A,B,D	https://archive.ics.uci.edu/ml/datasets/census+income
<i>covertypes</i> [10]	481k/100k	A,D	https://archive.ics.uci.edu/ml/datasets/covertypes
<i>credit</i> [90]	264k/20k	A,B,D	https://www.kaggle.com/mlg-ulb/creditcardfraud
<i>intrusion</i> [26]	394k/100k	A,D	http://archive.ics.uci.edu/ml/datasets/kdd+cup+1999+data
<i>mnist12</i> [45]	60k/10k	A,D	http://yann.lecun.com/exdb/mnist/index.html
<i>mnist28</i> [45]	60k/10k	A,D	http://yann.lecun.com/exdb/mnist/index.html

B.3 Image Data

We present results from an extra experiment on the *mnist28* dataset, this time benchmarking against a conditional GAN with convolutional layers [57]. We see in Fig. 4 that the cGAN clearly outperforms FORGE. This result is expected, given that our method is not optimized for image data. It also illustrates a limitation of our method, which excels in speed and flexibility but is no match for deep learning methods on structured datasets.

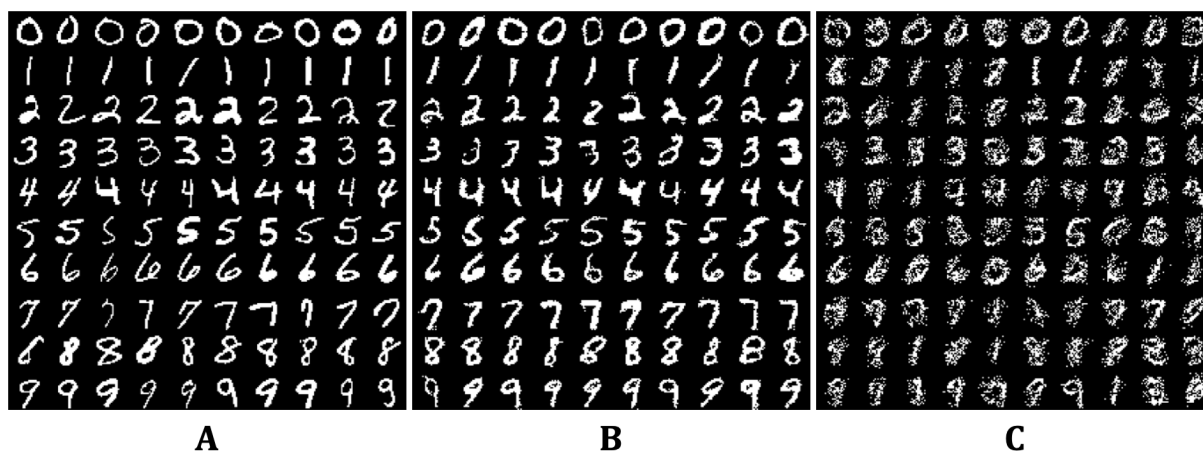


Figure 4: Results from *mnist28* experiment. (A): Original samples. (B): Samples generated by cGAN. (C): Samples generated by FORGE.

⁴https://sdv.dev/SDV/api_reference/tabular/ctgan.html. MIT License.

⁵https://sdv.dev/SDV/api_reference/tabular/tvae.html. MIT License.